Optical properties of size fractions of suspended particulate matter in littoral waters of Quebec

Gholamreza Mohammadpour[1], Jean-Pierre Gagné[1], Pierre Larouche[2], Martin A. Montes-Hugo[1*]

[1]Institut des Sciences de la Mer de Rimouski, 310 Alleé des Ursulines, Office P-216, Rimouski, Québec, Canada, G5L 3A1

[2]Institut Maurice-Lamontagne, Pêches et Océans Canada, Mont-Joli, Québec, Canada, G5H 3Z4

Correspondence to: Martin A. Montes-Hugo (martinalejandro_montes@uqar.ca)

Abstract. Empirical mass-specific absorption ($a_i^*(\lambda)$) and scattering ($b_i^*(\lambda)$) coefficients were derived for four size fractions (i = 0.2-0.4 μm, 0.4-0.7 μm, 0.7-10 μm, and >10 μm, λ = wavelength in nm) of suspended particulate matter (SPM) and with samples obtained from surface waters (i.e., 0-2 m depth) of the Saint Lawrence Estuary and Saguenay Fjords (SLE-SF) during June of 2013. For the visible-near-Infrared spectral range (i.e., λ = 400-710 nm), mass-specific absorption coefficients of total SPM (i.e., particulates > 0.2 μm) (hereafter a_{SPM}^*) had low values (i.e., 0.01-0.02 $m^2\ g^{-1}$) in areas of the lower estuary dominated by particle assemblages with relatively large mean grain size and high particulate organic carbon and chlorophyll a per unit of mass of SPM. Conversely, largest a_{SPM}^* values (i.e., > 0.5 $m^2\ g^{-1}$) corresponded with locations of the upper estuary and SF where particulates were mineral-rich and/or their mean diameter was relatively small. The variability of two optical proxies (the spectral slope of particulate beam attenuation coefficient and mass-specific particulate absorption coefficient, hereafter γ and *Svis*, respectively) with respect to changes on particle size distribution (PSD) and chemical composition was also examined. The power-law exponent of the exponential fit to the differential particle size distribution had a larger correlation with b_i^* estimates computed at a wavelength of 550 nm (Spearman rank correlation coefficient ρ_s up to 0.37) as opposed to a_i^* estimates derived at a wavelength of 440 nm (ρ_s up to 0.32). Conversely, the contribution of particulate inorganic matter to total mass of SPM (F_{SPM}^{PIM}) had a stronger correlation with a_i^* coefficients as derived at a wavelength of 440 nm (ρ_s up to 0.50). The magnitude of γ was positively related to changes of weight contributions of different size fractions of SPM (ρ_s up to 0.53 for i = 0.2-0.4 μm). Also, the relation between γ and F_{SPM}^{PIM} variability was secondary (ρ_s = -0.34, $P > 0.05$). Lastly, the magnitude of *Svis* was inversely correlated with $a_{SPM}^*(440)$ (ρ_s = -0.55, $P = 0.04$) and F_{SPM}^{PIM} (ρ_s = -0.62, $P = 0.018$) in sampling locations having a larger marine influence (i.e., lower estuary).

1 Introduction

The distribution of suspended particulate matter (SPM) (Table 1) in coastal and estuarine environments has a major influence on several biogeochemical processes (e.g., phytoplankton blooms) (Guinder et al., 2009), ecosystem structure (e.g., food webs) (Dalu et al., 2016) and dispersion of pollutants (e.g., copper, mercury, polycyclic aromatic hydrocarbons) (Ma et al., 2002; Ramalhosa et al., 2005). Light absorption by suspended particulates is essential for several photochemical processes related to the carbon cycle (e.g, photosynthesis, production of dissolved inorganic and organic carbon) (Estapa et al., 2012). Lastly, the concentration of SPM is an important variable for modeling thermodynamic processes and computing heat budgets (Löptien and Meier, 2011) due to its influence on underwater light attenuation (Morel and Antoine, 1994; Devlin et al., 2008).

The spatial and temporal variability of suspended particulates is relatively high (i.e., >100-fold) in littoral environments (Doxaran et al., 2002; Montes-Hugo and Mohammadpour, 2012). This represents a challenge for traditional methods of measuring SPM based on gravimetry (Strickland and Parson, 1972) as the analysis of a large number of samples is time-consuming and costly. Thus, these studies are commonly based on a relatively small dataset that may partially represent the in situ distributions of SPM. Due to these difficulties, several techniques have been developed for synoptic and large-scale mapping of SPM based on satellite-derived optical measurements (Doxaran et al., 2002; Miller and McKnee, 2004; Montes-Hugo and Mohammadpour, 2012).

SPM is an unknown mixture of inorganic and organic matter that varies between locations and as a function of time due to diverse physical (e.g., tides) and biogeochemical (e.g., phytoplankton growth) factors (D'Sa et al., 2008; Eleveld et al, 2014). Thus, optical remote sensing algorithms for estimating SPM are more region-specific and generally less accurate than those conceived for estimating specific fractions of SPM (e.g., particulate inorganic matter or PIM). This highlights the need for a better understanding of optical properties of SPM components that can be later used for estimating second-order attributes of SPM (i.e., chemical composition, size distribution) and designing more general remote sensing algorithms for retrieving total concentrations of particulates per unit of volume and across different water types.

In general, four techniques have been proposed for characterizing particle size distribution (PSD) and/or chemical composition of SPM based on optical measurements: (1) optical proxies (e.g., the spectral slope of particulate beam attenuation, γ, mass-specific absorption, *Svis*, and backscattering coefficients) (Boss et al., 2001; Loisel et al., 2006; Estapa et al., 2012), (2) mass-specific optical coefficients (e.g., mass-specific particulate scattering, backscattering and beam attenuation coefficients) (Bowers et al., 2009;Neukermans et al., 2012), (3) particulate volume scattering functions (Zhang et al., 2014), and (4) water leaving polarized reflectance (Loisel et al., 2008).

The Saint Lawrence Estuary (SLE) and the Saguenay Fjords (SF) constitute a large sub-Arctic system characterized by relatively high concentrations of chromophoric dissolved organic matter (CDOM) (Nieke et al., 1997). The remote sensing of physical attributes of SPM (e.g., PSD) in these waters is crucial for studying regional climate effects on coastal erosion and occurrence of harmful algae blooms. However, in order to accomplish this task it is essential to know how optical characteristics of suspended particulates (e.g., mass-specific optical coefficients) are influenced by particle composition and

size distribution changes. To our knowledge, mass-specific absorption and scattering coefficients of SPM size fractions have never been reported in the literature even though it has a potential application in biogeo-optical modeling and biogeochemical studies regarding the dynamics of trace metals, sediment transport and primary productivity models.

This study has three main objectives: (1) to characterize the mass-specific absorption ($a_i^*(\lambda)$) and scattering ($b_i^*(\lambda)$) coefficients of four size fractions of SPM (i = 0.2-0.4 µm, 0.4-0.7 µm, 0.7-10 µm, and >10 µm, λ = wavelength in nm) at different locations of the SLE-SF and during spring conditions, (2) to establish relationships between mass-specific optical coefficients calculated in (1) and characteristics of particle assemblages related to PSD and mineral content of SPM, and (3) to examine the correlation between optical proxies γ and *Svis*, and variables linked to PSD and chemical composition of SPM..

This study is organized in three sections. In the first section, mass-specific absorption (a_{SPM}*) and scattering (b_{SPM}*) coefficients of total SPM (i.e., particulates >0.2 µm) are calculated for different optical environments of the SLE-SF that are characterized by distinct particle assemblages and variable contributions of CDOM, non-algal particulates (NAP) and phytoplankton to light attenuation. In the second section, relationships between mass-specific optical coefficients of different SPM size fractions and parameters related to PSD and mineral-content of suspended particulates are investigated. Lastly in the third section, relationships between optical proxies γ and *Svis* and second-attributes of SPM linked to particle chemical composition and PSD are analyzed.

2 Data and methods

2.1 Study area

The SLE can be divided in two main regions having contrasting biological productivity and bathymetry: the upper (UE) and the lower (LE) estuary (Levasseur et al., 1984). NAP and CDOM dominate the diffuse light attenuation of SLE waters (Nieke et al., 1997). This is partially related to the inflow of CDOM-rich and NAP-rich waters coming from the St. Lawrence River and Saguenay Fjord (Tremblay and Gagné, 2007; Xie et al., 2012). Unlike NAP and CDOM, contribution of phytoplankton to inherent optical properties increases towards the mouth of the SLE (Montes-Hugo and Mohammadpour, 2012; Xie et al., 2012).

The study of optical properties of suspended particulates in SLE waters began during the late 80's. Babin et al. (1993) investigated the horizontal variability of the specific absorption coefficient of phytoplankton (i.e., absorption coefficient normalized by concentration of chlorophyll + phaeopigments) in surface waters during summer of 1989 and 1990. During the summer of 1990, Nieke et al. (1997) reported for the first time relatively high values (up to 3 m^{-1}) of particulate beam attenuation coefficients (c_{SPM}) and inverse relationships between salinity, c_{SPM}, and CDOM absorption coefficients (a_{CDOM}). Larouche and Boyer-Villemaire (2010) proposed remote sensing models for estimating PIM in the SLE and the Gulf of Saint Lawrence. Xie et al. (2012) showed inverse relationships between salinity and absorption coefficients of NAP and highlighted the extremely high values of a_{CDOM} (i.e., up to 5.8 m^{-1} at λ = 412 nm) along the Saguenay Fjord.

Historical studies performed during summer of 1975 suggest that size distribution of SPM differs between UE, LE and SF subregions (Poulet et al., 1986). Based on surface samples, Poulet et al. (1986) found a dominance of relatively 'small-sized' (i.e., mode diameter < 10 μm) and 'large-sized' (i.e., > 30 μm) particulates over the UE and the mouth of the SLE, respectively. Conversely, the remaining locations of the LE were characterized by particulates having an intermediate size. In surface waters of SF and during spring, Chanut and Poulet (1982) found that SPM is commonly composed by very small particles (i.e., 2-3 μm). Several investigations point out that suspended particulates in SLE-SF regions are principally composed by inorganic matter (D'Anglejan and Smith, 1973; Larouche and Boyer-Villemaire, 2010; Mohammadpour et al., 2015). This mineral contribution may vary between 60 and 95% of dry weight depending on the geographic location and period of the year (Yeats, 1988; Larouche and Boyer-Villemaire, 2010).

Despite their important contribution to the study of physical and chemical properties of SPM, none of these studies investigated relationships between chemical composition, size distribution, mass-normalized optical coefficients and optical proxies of second-order attributes of SPM.

2.2 Field surveys

Discrete water samples for biogeochemical and optical measurements were obtained in 22 locations distributed throughout the SLE (N =17) and SF (N = 5) regions (Fig. 1). One discrete sample was obtained in each sampling locations but in site 6 where 2 measurements were made during June 3 and 6 of 2013. Surface samples (i.e., 0-2 m depth) were collected during June 3-9 of 2013 by using an oceanographic rosette equipped with Niskin bottles (volume = 12 L). For each study location, PSD of unfractionated water samples, and optical properties of different size fractions of SPM were determined onboard of the ship.

2.3 Biogeochemical analysis

Size fractionation of SPM was done after sequentially filtering the original samples through pre-weighted membranes having a diameter of 47 mm and a pore size of 10 μm (Whatman, polycarbonate), 0.7 μm (GF/F, Whatman, glass fiber), 0.4 μm (Whatman, polycarbonate), and 0.2 μm (Nucleopore, polycarbonate). The contribution of size fraction i to the total mass of SPM (F_{SPM}^{i}, i = 0.2-0.4 μm, 0.4-0.7 μm, 0.7-10 μm, and >10 μm) was computed by normalizing the weight of the fraction i by the sum of weights derived from each size fraction. The contribution of PIM to total mass of SPM (F_{SPM}^{PIM}) was only computed for particulates with a grain size greater than 0.7 μm (i.e., after filtering the original unfractionated sample trough a GF/F filter membrane). In this case, the mass of PIM and particulate organic matter (POM) was assumed to be negligible for particulates with a diameter smaller than 0.7 μm. This approximation should be verified in the future since the authors are not aware of publications addressing the contribution of relatively small particulates (i.e., < 0.7 μm) to PIM and POM. The mass of PIM was obtained after removing the organic mass by combustion of original samples at 450°C and during 6 h (Mohammadpour et al., 2015). The mass of POM was calculated as the difference between the dry mass of SPM concentrated in GF/F filters minus the dry mass of PIM.

The precision of SPM mass determinations based on GF/F filters was 15% (Mohammadpour et al., 2015). This precision was computed as the percentage of ± 1 standard deviation with respect to the arithmetic average of weight corresponding to 10 replicas. Based on loss on ignition factors (Barillé-Boyer et al., 2003) and clay composition data obtained in the Saint Lawrence Estuary (D'Anglejan and Smith, 1973), the estimated error of PIM determinations due to dehydration of clays was 3.1%. Thus, PIM mass determinations have a maximum uncertainty of 18.1% due to the additional error of SPM mass measurements. Notice that error in POM mass estimates was slightly greater than that associated to PIM mass estimates (18.2%).

2.4 Optical measurements

Total absorption (a) and beam attenuation (c) coefficient measurements were done on unfractioned and size-fractioned water samples previously described in section 2.3. Discrete samples for optical coefficients were measured by using an absorption-beam attenuation meter (ac-s, WetLabs, λ = 400.3-747.5 nm, average spectral resolution = 4 nm, path-length = 10 cm, accuracy ± 0.001 m^{-1}). In order to minimize the presence of bubbles, a pump (ISMATEC MCP-Z) was used to gently circulate the samples during the measurements. Spikes on raw signal associated to bubbles were removed by visual inspection. The residual scattering on absorption measurements was removed by applying a flat baseline at a reference wavelength of 715 nm (Bricaud and Stramski, 1990). This is a first order correction for scattering effects on non-water absorption coefficient estimates. Thus, the calculation of particulate absorption coefficients in this study is expected to have a bias with respect to true values measured using absorption-meter instruments that are less influenced by particulate scattering (e.g., point-source integrating-cavity absorption meters) (Röttgers et al., 2013). Lastly, values of a and c were corrected by water temperature and salinity variations (Pegau et al. 1997). Spectral values of a_{SPM} in m^{-1} were derived from unfractionated samples by subtracting the contribution of CDOM and pure seawater to a. The magnitude of a_{CDOM} was determined after pre-filtration of size-fractionated samples through a membrane having a pore size of 0.2 µm (nucleopore, Whatman). Similar to a_{SPM} calculations, values of c_{SPM} were derived from unfractioned samples after subtracting CDOM and pure seawater contributions to c. Lastly, particulate scattering coefficients (b_{SPM}) in m^{-1} were derived by subtracting a_{SPM} to c_{SPM} values. Notice that pure seawater contributions to a and c values are initially removed when the ac-s instrument is calibrated by the manufacturer. Seawater absorption and scattering coefficients are derived from tables (Morel, 1974; Pope and Fry, 1997).

Bench determinations of PSD were made by using a red laser (wavelength = 670 nm) diffractometer (LISST-100X, type B, Sequoia Scientifics) (Agrawal et al. 1991). Lab measurements were performed by using a chamber and a magnetic stir bar in order to homogenize the samples and avoid sinking of particulates. The optical path was covered with a black cloth to minimize ambient light contamination during the scattering measurements. The LISST-100X instrument can measure 32 scattering angles within an angular range of 0.08-13.5°, thus, particulates with a diameter between 1.25 and 250 µm can be quantified. However only the interval 3-170 µm was analyzed due to stray light effects and variability of particle shape and refractive index in the first bins (i.e., < 3.2 µm) (Agrawal et al., 2008; Andrews et al., 2010; Reynolds et al. 2010), and bias related to particle sinking in the last bins (i.e., 170-250 µm) (Reynolds et al. 2010). The Hampel filter algorithm was applied to the

original measurements in order to eliminate potential outliers (Pearson, 2005). Lastly, each final PSD estimate was computed as the average of measurements made during 3 minutes at 1 Hz sampling rate.

The number of particles per unit of volume within each size class (N(D)) was computed by dividing the particle volume concentration (V(D)) by the diameter (D) of a volume-equivalent sphere corresponding to the midpoint of each individual class:

$$N(D) = 6\ V(D)\ (\pi\ D^3)^{-1} \quad (1)$$

A total of 25 particle size bins were calculated from scattering patterns of spherical homogenous particles as predicted from Mie theory and a realistic range of index of refraction. The particle size distribution (N'(D)) was defined as the average number of particles within a given size class of width ΔD and per unit of volume (Reynolds et al., 2010):

$$N'(D) = N(D)\ \Delta D^{-1} \quad (2)$$

The power-law exponent of the exponential fit to the differential PSD (ξ) was computed as follows:

$$N'(D) = N'(Do)\ (D/Do)^{-\xi} \quad (3)$$

where Do is the reference particle diameter and was set to the midpoint of the size logarithmic size range (i.e., 35.17 μm). Calculations of ξ were done by least square minimization of log-transformed data (Reynolds et al., 2010). The uncertainty of ξ calculations, as estimated from 2 standard errors, varied between 1.6 and 10.2% with smaller errors in samples obtained in LE locations. Although PSD in natural waters may not follow the model proposed in equation (3), its use here was justified as our main interest was to have a first-order assessment of size effects of particulates on optical coefficient's variability. Also, the definition of ξ based on LISST measurements applies for particulates greater than 2 μm. A more realistic representation of PSD is the model proposed by Risovic (1993). This parameterization mainly includes two particle populations ('large' and 'small') having different refractive index and has been recently applied in littoral environments by different studies (Zhang et al., 2013; Zhang et al., 2014; Zhang et al., 2017). Thus, relationships between ξ and optical coefficients in this study are local and should not be generalized to other littoral environments.

2.5 Optical proxies and characteristics of particle assemblages

A widely used methodology for estimating size spectra of suspended particulates is the calculation of γ (Boss et al., 2001). The parameter γ is positively correlated with the power-law exponent fit to the particle number size distribution (ξ) ($\xi = \gamma + 3 - 0.5\ e^{-6\gamma}$) (Boss et al., 2001) and negatively related with the mean particle size for particles smaller than 20 μm (Boss et al., 2013). The parameter γ was derived as follows:

$$c_{SPM}(\lambda) = c_{SPM}(488)\ (\lambda/\lambda r)^{-\gamma} \quad (4)$$

where λr is the reference wavelength at 488 nm (Boss et al., 2013).

The uncertainty of γ determinations varied between 2.2% and 6.4% with largest errors computed in samples obtained in LE waters. The spectral slope of mass-specific particulate absorption coefficients (*Svis*) was calculated by nonlinear fitting of a single-exponential decay function over the visible range 400-700 nm:

$$a_x^*(\lambda) = A\, e^{-Svis\,(\lambda-400)} + B \quad (5)$$

where x corresponds to total SPM or the size class i, the term *B* corresponds to an offset at near-IR wavelengths to account for nonzero absorption by mineral particles (Babin et al. 2003; Röttgers et al., 2014). The uncertainty of *Svis* estimates varied between 0.5 and 21.5% with largest errors associated to samples obtained in LE locations. The equation (5) is only valid in waters where non-algal particulates are the main optical component contributing to light absorption coefficient of SPM.

2.6 Mass-specific optical coefficients

The spectral mass-specific absorption ($a_i^*(\lambda)$) and scattering ($b_i^*(\lambda)$) coefficients in $m^2\ g^{-1}$ and for different size fractions of SPM are defined as follows:

$$a_i^*(\lambda) = a_i(\lambda)\ (wp_i)^{-1} \quad (6)$$

$$b_i^*(\lambda) = b_i(\lambda)(wp_i)^{-1} \quad (7)$$

For each size class i, a_i and b_i are the coefficients of particulate absorption and scattering, respectively, and wp_i is the mass of particulates per unit of volume in $g\ m^{-3}$.

2.7 Statistical analysis

Relationships between PSD,, particle chemical composition, optical proxies (γ and *Svis*) and empirical mass-specific optical coefficients for different size fractions (i.e., a_i^* and b_i^*) of SPM were investigated based on correlations with respect to ξ and F_{SPM}^{PIM} variables. In all cases, the intensity and sign of correlations were quantified based on non-parametric Spearman rank coefficient (ρ_s) (Spearman, 1904).

3 Results

3.1 Spatial variability of physical and chemical characteristics of SPM

The size distribution of particulates presented contrasting changes among different subregions of the study area. In general, particulates with a diameter larger than 10 μm had a relatively large contribution to the total SPM mass in UE locations ($F_{SPM}^{>10\ \mu m}$ as percentage up to 17%). This proportion was lower in the LE (up to 11%) and SF (up to 15%) subregions. The largest mass contribution of smallest-sized particulates (i.e., diameter < 0.4 μm) was calculated in the lower estuary (up to 27%). Lastly, the intermediate size classes 0.4-0.7 μm and 0.7-10 μm were in average the fractions having the largest mass contributions to SPM in SF locations (up to 14 and 87%, respectively). In general, the magnitude of ξ suggested the presence of larger particulates in the LE (arithmetic average ± standard deviation = 3.28 ± 0.38, N = 15) with respect to UE (3.46 ± 0.36, N = 3) and SF (3.42 ± 0.39, N = 5) subregions. Unlike PSD, the mineral content of SPM was less variable throughout the study area (F_{SPM}^{PIM} range = 37 to 87 %). In average, particle chemical composition in UE, SF and LE subregions was dominated by minerals (F_{SPM}^{PIM} = 0.65 ± 0.13, 0.67 ± 0.14 and 0.67 ± 0.14 for SF, UE and LE, respectively).

3.2 Mass-specific optical coefficients of particulates

In general for the visible spectrum, the subregional average of mass-specific absorption particulate coefficients was higher in SF (e.g., $a_{SPM}^*(440) = 0.523 \pm 0.102$ m^2 g^{-1}, arithmetic average ± standard error) with respect to UE (0.122 ± 0.069 m^2 g^{-1}) and LE (0.062 ± 0.010 m^2 g^{-1}) locations (Fig. 2a). Conversely, the subregional average of mass-specific particulate scattering coefficients was comparable between different spatial domains of the SLE (Fig. 2b). However, the highest and lowest values subregional averages of b_{SPM}^* tended to be associated with UE (e.g., $b_{SPM}^*(440) = 0.499 \pm 0.278$ m^2 g^{-1}) and LE (0.181 ± 0.046 m^2 g^{-1}) locations, respectively. In general for all size fractions of SPM, mass-specific absorption coefficients were usually higher in SF (e.g., $a_i^*(440)$ up to 2.81 m^2 g^{-1}) with respect to UE and LE subregions (up to 2.11 m^2 g^{-1}) (Fig. 3). However, this pattern was reversed when the grain size of particulates was smaller than 0.4 μm (Fig. 3a). Indeed, the highest $a_{0.2\text{-}0.4\ \mu m}^*$ estimates in this study corresponded to UE waters (e.g., st 14) (2.19 m^2 g^{-1}) (Fig. 3a).

In general, very high a_i^* values (e.g., up to 4 m^2 g^{-1} at $\lambda = 400$ nm) were associated with the size fraction of SPM having particulates with a diameter greater than 10 μm (Fig. 3d). These values were up to 8 and 5 times higher than those characteristic of size fractions 0.4-0.7 μm and 0.7-10 μm, respectively (Fig. 3b-c). In general, ξ and F_{SPM}^{PIM} correlations with mass-specific absorption coefficients of different size fractions of SPM suggest that particle chemical composition has a larger influence on $a_i^*(440)$ (ρ_s up to 0.50, $P = 0.0009$) with respect to PSD (ρ_s up to 0.32, $P = 0.0033$) (Table 2).

Similar to a_i^*, highest b_i^* values (up to 5.70 m^2 g^{-1} at $\lambda = 400$ nm) were associated with particulates within two size ranges, 0.2-0.4 μm and >10 μm (Fig. 4). Notice that mass-specific optical coefficients in the near-Infrared (NIR) spectral range are not shown due to the presence of negative values at some wavelengths. For the same size range of particulates, the highest b_i^* values were not always measured in the same region. Indeed, maximum b_i^* values for the size fractions 0.7-10 μm (up to 1.25 m^2 g^{-1} at $\lambda = 556$ nm) and >10 μm (up to 4.58 m^2 g^{-1}) were obtained in UE and LE domains, respectively. Unlike $a_i^*(440)$, $b_i^*(550)$ variability was less influenced by changes on particle composition (ρ_s up to 0.42, $P = 0.0015$) (Table 2). Conversely, the impact of changing particle dimensions, as inferred from ρ_s correlations, had a larger effect on $b_i^*(550)$ (ρ_s up to 0.37, $P = 0.006$) with respect to $a_i^*(440)$ (ρ_s up to 0.32, $P = 0.009$) values.

The spectral variability of mass-specific optical coefficients for two size fractions of SPM and averaged over the whole study area is illustrated in Fig. 5. For the spectral range of 440-556 nm, a_i^* values for the size range 0.2-0.4 μm tended to be higher with respect to those associated with particulates larger than 10 μm (Fig. 5a). Conversely, this trend appeared to be reversed at wavelengths within the red-NIR spectral range. In general for the visible-NIR wavelengths, the arithmetic average of b_i^* for the size fraction 0.2-0.4 μm were consistently larger with respect to that associated to the size fraction >10 μm (Fig. 5b).

3.3 Optical proxies

Correlations between size and chemical fractions of SPM as derived from mass ratios, and optical proxies are presented in Table 3. Over the whole study area, there was not a clear relationship between γ and F_{SPM}^{PIM} values ($\rho_s = -0.34$, $P = 0.11$).

However, γ changes were associated to variations of size-fractionated mass contributions of particulates within the range 0.2-10 μm (ρ_s up to 0.53, P = 0.01). The sign of this correlation varied depending on the size class under investigation (e.g., positive and negative ρ_s values for small-sized and intermediate-sized particulates, respectively). There was not a clear relationship between γ and ξ values calculated with samples obtained over the whole study area (ρ_s = 0.15, P = 0.49, N = 23). The range of γ values was 0.759-3.282, 1.389-1.534, 2.873-3.282 and 0.759-1.802 nm^{-1} for the SLE, UE, SF and UE domains, respectively. The spectra slope of a_{SPM}^* was not statistically related to F_{SPM}^{PIM} changes (ρ_s = -0.06, P = 0.78, N = 23). However *Svis* variability was strongly connected with changes on mass contribution of different size classes of SPM ,and in particular those associated to small-sized particulates (i.e., 0.2-0.7 μm) (Table 3). This pattern was consistent with a positive correlation between γ and *Svis* (ρ_s = -0.489, P = 0.018, N = 23). However, there was not a clear relationship between *Svis* and ξ values (ρ_s = 0.123, P = 0.57, N = 23).

The range of *Svis* values for unfractionated samples of SLE-SF, UE, SF and UE domains was 0.005-0.051, 0.009-0.017, 0.014-0.051 and 0.005-0.016 nm^{-1}, respectively. Over the whole study area, the range of *Svis* values for SPM size fractions 0.2-0.4 μm, 0.4-0.7 μm, 0.7-10 μm and > 10 μm was 0.004-0.026, 0.007-0.052, 0.004-0.109 and 0.001-0.028 nm^{-1}, respectively. In general, *Svis* slopes were not correlated between size fractions even though the variation of *Svis* for unfractionated samples was strongly linked to changes on *Svis* estimates associated to particulates within the size range 0.7-10 μm (ρ_s = 0.66, P = 0.004).

4 Discussion

4.1 Uncertainty of optical measurements

Inherent optical properties in this study were derived from an ac-s instrument. Thus, large errors on absorption coefficients may be anticipated in relatively turbid waters if original measurements are not corrected by scattering effects (Boss et al., 2009; McKee et al., 2013). These effects are mainly attributed the acceptance angle of the transmissometer and the multiple scattering of photons. The acceptance angle of the ac-s instrument is ~0.9° and much larger than that corresponding to the LISST-100X diffractometer (~0.027°). Thus, a larger underestimation on *c* magnitude is expected in ac-s with respect to LISST-100X measurements due to a larger contribution of forward-scattered photons arriving to the detector of the former optical instrument. Further comparisons of *c*(532) measurements derived here by ac-s and LISST-100X showed that *c* values as derived from ac-s were 23-84% lower with respect to those determinations based on LISST-100X. This is consistent with Boss et al. (2009) who reported that uncorrected Wet Labs ac-9 attenuation values are approximately 50%-80% of equivalent LISST attenuation data. Unfortunately, *c* deviations due to acceptance angle variations were not corrected in this study due to the lack of true *c* values as obtained by using an integrating cavity absorption meter (e.g., PSICAM) (Röttgers et al., 2005). Notice that these errors are much greater with respect to the standard deviation of each sample determination in this study and computed based on ac-s measurements (e.g., < 1% at λ = 532 nm).

In this investigation, the 'flat' baseline correction was selected for correcting the residual scattering in absorption coefficient estimates as derived from ac-s measurements. This technique was chosen due to the lack of PSICAM measurements or ancillary optical information (e.g., particle backscattering efficiency) to tune up a Monte Carlo scattering correction approach (McKee et al., 2008). The 'flat' scattering correction approach is expected to provide a fair correction of a values in oceanic waters (e.g., up to 15% underestimation at wavelengths shorter than 600 nm, see Fig. 8b, McKnee et al., 2013) but may result in large deviations (e.g., up to 100% decrease in the NIR spectral range) of a values in relatively turbid waters (e.g., $a > 0.2$ m^{-1}) such as the Baltic/North Sea. Also, this issue is present when the proportional correction method of Zaneveld et al. (1994) is applied. Unlike the 'flat' baseline, the scattering residual of the proportional method is spectrally dependent but still relying in one reference wavelength in the NIR spectral range. Approximations justifying the use of the 'flat' (i.e., zero absorption signal in the NIR) and 'proportional' (i.e., wavelength-dependent scattering phase function) method are still in debate (McKnee et al., 2013). Lastly, the Monte Carlo correction method (McKee et al., 2008) has in general a better agreement (error <10%) with true a values as derived from an integrating cavity absorption meter. However, this approach may also have major uncertainties due to assumptions regarding optical coefficients (e.g., particulate backscattering ratio and volume scattering function) and changes on scattering efficiency due to factors related to the optical instrument (e.g., aging of the reflective tube of the absorption-attenuation meter) (McKnee et al., 2013). Thus in conclusion, the resulting optical coefficients and mass-specific optical coefficients of particulates measured in SLE-SF waters may present large errors (i.e., > 50%) with respect to true values and at wavelengths longer than 550 nm. This bias is anticipated to be maximum (minimum) in UE (LE) locations.

4.2 Variability of physical and chemical characteristics of SPM

A striking finding in this study was the important weight contribution of relatively large particulates (i.e., >10 μm) to the total mass of SPM in UE waters. This phenomenon was likely attributed to the active resuspension of sediments associated with vertical mixing produced by tidal currents and winds (Yeats, 1988). Conversely, this effect was secondary in relatively deep waters of SF and LE where large and heavy particulates are rapidly removed from the water column and deposited along submarine canyons (Gagné et al., 2009). The chemical composition of size-fractioned SPM was not analyzed in this study. However, additional correlations between F_{SPM}^{PIM} and $F_{SPM}^{0.2\text{-}0.7\ \mu m}$ values suggest that mineral content of SPM increases as the contribution of particulates with a diameter smaller than 0.7 μm becomes larger ($\rho_s = 0.30$, $P = 0.035$, N = 23).. This finding is consistent with previous studies in the SLE showing that relatively small (i.e., diameter ~2 μm) particulates are mainly composed by inorganic matter (Yeats, 1988; Gagné et al., 2009). In this contribution, a large proportion of particulates with a diameter above 50 μm and lower ξ values were typically found in LE locations. These results go along with historical datasets and showing a greater proportion of relatively large particulates (i.e., > 5 and < 50 μm) over the LE locations and during the same period of the year (Chanut and Poulet, 1982).

4.3 Spatial variability of mass-normalized optical coefficients

In this study, a_{SPM}^* measurements in the visible and near-IR range had a large variability that was comparable to the range of values reported in the literature for temperate coastal waters (e.g., Mobile Bay, Elbe Estuary, Gironde Estuary) (Stavn and Richter, 2008; Doxaran et al., 2009) (Table 4). This is remarkable given the large diversity of methodologies used by different research teams for estimating a_{SPM}^* values. In general, the lowest a_{SPM}^* values (i.e., 0.01-0.02 $m^2\ g^{-1}$ at $\lambda = 440$ nm) commonly corresponded with samples obtained in very turbid environments (i.e., > 100 $g\ m^{-3}$, Mississippi River and Delta, Gironde River) (Bowers and Binding, 2006; D'Sa et al. 2006; Doxaran et al., 2009). Notice that part of this decrease can be attributed to an incomplete removal of multiple scattering effects. Relative low a_{SPM}^* values have been linked to high POC/SPM (Wozniak et al., 2010) and chl/SPM concentration ratios, where chl means chlorophyll a concentration (Estapa et al., 2012). In this study, chl/SPM values are relatively high (up to as 2 10^{-3}) with respect to those reported in the literature (~10^{-3}) (D'Sa et al., 2006) and are consistent with low a_{SPM}^* estimates.

A well-known mechanism explaining the general decrease of a_{SPM}^* in very turbid waters is related to packaging effects (Morel, 1974; Zhang et al., 2014). At higher turbidities, larger particulates contribute to PSD variations, thus as mean diameter of particles increases, the light absorption efficiency per averaged particle decreases (i.e., the interior of larger particles has a greater 'shading'). This could also explain the spatial differences of $a_{SPM}^*(440)$ in our study area where larger values corresponded with surface waters dominated by particles assemblages having a smaller mean diameter (e.g., UE and SF). In nearshore waters of California, Wozniak et al. (2010) demonstrated inverse relationships between $a_{SPM}^*(440)$ and the median particle diameter of inorganic- and organic-dominated assemblages.

Indirect size effects on $a_{SPM}^*(440)$ due to changes on iron content per particle have been discussed by Estapa et al. (2012) in environments where optical properties are dominated by NAP. In general, smaller particulates have a greater surface for adsorbing organic compounds where iron can accumulate (Mayer, 1994; Poulton and Raiswell, 2005). Thus, SPM fractions with small-sized particulates are expected to have an enhancement of $a_{SPM}^*(440)$ due to relatively high iron concentrations. This phenomenon could probably explain part of the $a_{SPM}^*(440)$ variability in some locations of our study area where relatively high concentrations of iron bound to particulates have been measured (e.g., SF) (Yeats and Bewers, 1976; Tremblay and Gagné, 2009).

Similar to a_{SPM}^*, b_{SPM}^* values were highly variable between locations and within the range of measurements obtained in other environments (Table 4). In this study, the spectral variation b_{SPM}^* between regions showed a spectral flattening as particle assemblages become dominated by organic matter (i.e., LE). This finding is consistent with Wozniak et al. (2010) determinations made in Imperial Beach, California.

4.4 Relationships between PSD, particle chemical composition and mass-specific optical coefficients

For all size fractions of SPM, ξ was positively correlated with $a_i^*(440)$ (ρ_s up to 0.32, $P = 0.006$). This pattern suggests a higher absorption efficiency of relatively small-sized particulates. As previously discussed, these particulates have a greater light

absorption per unit of particle mass due to a lesser role of shading effects. Since particle aggregates were altered during our experiments, the influence of particle density on mass-specific optical coefficients cannot be quantified as this effect is mainly observed in undisrupted marine aggregates (Slade et al. 2011; Neukermans et al., 2012, Neukermans et al 2016). However and based on Estapa et al. (2012) simulations, the impact of aggregation on a_{SPM}^* is anticipated to be small (i.e., ~10%) with respect to the spatial variability of a_{SPM}^* in SLE-SF waters (>500%).

In general, ξ was positively correlated with $b_i^*(550)$ (ρ_s up to 0.37, $P = 0.008$) and suggests an increase of scattering efficiency as particulates become smaller and the influence of packaging effects is less important. Notice that ξ correlations with $b_i^*(550)$ were greater with respect to $a_i^*(440)$ and more remarkable for relatively large-sized particulates. In Arctic waters, Reynolds et al. (2016) observed an increase on mass-specific particulate backscattering for mineral-rich particle assemblages that tend to exhibit steeper PSDs. Although no particulate backscattering measurements were available in this study, Reynolds et al. (2016) highlight the importance of PSD for driving variations on mass-specific optical coefficients linked to scattering processes.

A common pattern in all size fractions of SPM was the stronger correlation of F_{SPM}^{PIM} with $a_i^*(440)$ compared with $b_i^*(550)$ values. The enrichment of suspended particulates on inorganic matter and concomitant variations $a_i^*(440)$ may be attributed to mineral-associated iron (Babin and Strasmki, 2004; Estapa et al., 2012) or/and organic-associated iron (Estapa et al., 2012)... Also, the combustion method used to measure PIM in our study could be another factor explaining the increased particle absorption in the blue range (Babin et al. 2003). In SF locations, reduced iron is mainly associated to dissolved organic compounds that can be strongly adsorbed to hydrous metal oxides (Deflandre et al., 2002).

An important objection to correlations of ξ and F_{SPM}^{PIM} with mass-specific optical coefficients of SPM for different size fractions was related to differences in terms of particle size range used to compute ξ and F_{SPM}^{PIM} and particle size classes derived by sequential filtration of water samples. More specifically, ξ is not representative of submicron particles less than 2 μm. Also, F_{SPM}^{PIM} is only a valid parameter for particles mostly larger than 0.7 μm. Thus, correlations ξ and F_{SPM}^{PIM} with mass-specific optical coefficients of 0.2-0.4 μm and 0.4-0.7 μm may only reflect indirect dependencies between mass-normalized optical coefficients of different size classes. This possibility (i.e., correlations between a_i^* or b_i^* values of different size classes) was confirmed *a posteriori* based on samples obtained in UE, LE and SF waters.

Lastly, it is important to discuss the potential bias on a_i^* and b_i^* determinations due to size fractionation and subsequent impact on correlations with respect to F_{SPM}^{PIM} and ξ values. No measurements of F_{SPM}^{PIM} and ξ were done in size fractions of SPM, thus it is difficult to compare PSD and particle chemical composition changes before and after the size fractionation of the samples. Size fractionation is anticipated to cause retention of smaller particulates in membranes having a larger pore size. These primary particles will overestimate the weight of the filtered sample and underestimate the weight of the next filtration step consisting in a membrane having a smaller pore size. Since particle sieving begins with large-sized particles and finishes with small-sized particles, the magnitude of a_i^* and b_i^* for relatively large (small) particulates is likely to be under-(over-) estimated. Bias on mass of particulates for each size fraction was verified by comparing the sum of weights of 0.7-10 μm and >10 μm fractions with the weight of an independent sample after filtering it through a GF/F membrane (i.e., 0.7 μm nominal

pore size). In this case, the arithmetic average (median) of the relative bias for the whole dataset was 29.7% (24.9%) or a 29.7% (24.9%) overestimation with respect to samples without a previous size fractionation.. An optimization scheme to adjust the mass for each size fractions (i.e. adjusting the various weights to sum up to the total mass filtered) was not attempted since we didn't filter unfractionated samples through 0.2 or 0.4 μm membranes due to the sequential mode of our filtration. Thus, 'filtration weighting factors' for size fractions > 0.2 μm or > 0.4 μm could not be calculated.

4.5 Optical proxies of SPM characteristics

In terms of fractioned mass, the size of particulates was the dominant variable driving changes on γ (ρ_s up to 0.53, $P = 0.004$). Conversely, the mineral content of SPM did not have a statistically detectable impact on γ at 95% confidence level. In particular, the strongest relationship betwen γ and F_{SPM}^{i} was associated to the fraction having the smallest particles (i.e., 0.2-0.4 μm). Despite the major effects of particle size classes on γ, values of γ were not clearly correlated with ξ values. In oceanic waters, ξ and γ values are expected to covary in a linear way for a specific range of refractive index and ξ (Boss et al., 2001; Twardowski et al., 2001). Our range of ξ values was within the natural variability reported in coastal and oceanic environments (ξ = 2-4.5) (Reynolds et al., 2010; Neukermans et al., 2012; Xi et al., 2014). Also, the magnitude of γ in our samples (0.29-2.22 nm^{-1}) was within the range of values that characterize oceanic environments (0.2-2) (Twardowski et al., 2001, Boss et al., 2013). Unlike oceanic waters, the poor correspondence between ξ and γ values in this study was linked to different relationships between γ, ξ and changes of two non-covarying optical contributions: minerals and phytoplankton. Also, the reduced number of sampling locations and the geographic variability of ξ-γ relationships were additional factors likely explaining the lack of correlation for the study area. Lastly, ξ and γ were not substantially correlated in our samples due to deviations on Mie-based models (e.g, absorbing spheres) of γ as a function of ξ (Twardowski et al., 2001). Indeed during our surveys, high absorbing particulates were present in SLE-SF waters.

The variability of *Svis* values in this study was relatively high (~10-fold) with respect to other littoral environments (1.3-fold, *Svis* = 0.009-0.0113 nm^{-1}) (Estapa et al., 2012). *Svis* was inversely related to $a_{SPM}^{*}(440)$ in surface waters of the SLE having a major marine influence (i.e., salinity range = 29-33.5, LE locations) (ρ_s = -0.55, $P = 0.04$, N = 14). In coastal waters of the Gulf of Mexico, Estapa et al. (2012) found that $a_{SPM}^{*}(440)$ (*Svis*) tends to increase (decrease) in iron-enriched particle assemblages of marine samples. Whether this phenomenon is also occurring in the SLE is unknown and should be investigated in future studies.

5 Conclusions

The measure of mass-specific optical coefficients of SPM is essential for developing optical inversions for mapping biogeo-chemical components in surface waters and improving our understanding regarding the origin of optical signatures in remote sensing studies. In this contribution, we presented for the first time, mass-specific scattering and absorption coefficients of size-fractioned SPM in estuarine waters of the Saint Lawrence River and a major SLE tributary, the Saguenay Fjord.

Despite the intrinsic variability of weight-normalized optical coefficients due to variations of physical and chemical properties of particle assemblages, the following patterns were identified: 1). the mass-specific absorption coefficient of different size fractions of SPM was preferentially related to changes on particle chemical composition as inferred from changes on F_{SPM}^{PIM} and at a wavelength of 440 nm, 2) the magnitude of ξ had a stronger correlation with $b_i^*(550)$ compared to $a_i^*(440)$, and 3) the magnitude of *Svis* was inversely correlated with $a_{SPM}^*(440)$ in areas having a larger marine influence (i.e., lower estuary). In summary, these relationships will be useful for investigating local and regionally-limited biogeo-optical properties of SPM. Thus, additional research based on true optical properties of PSD will be needed in order to propose more general relationships that can be applied to other littoral environments.

6 Funding

This investigation was supported by the Natural Sciences and Engineering Research Council of Canada, Individual Discovery grant, project title: "Optical remote Sensing models of suspended Particulate matter in the St. Lawrence Estuary "(OSPLE), awarded to Dr. Martin Montes Hugo.

7 Acknowledgements

We thank to the crew of the Creed and Mr. Alexandre Palardy for their assistance during the field work. Also, we appreciate the support of ISMER technicians Mr. Pascal Rioux and Ms. Dominique Lavallée during the field surveys and the processing of lab measurements. Lastly, we are really in debt with the constructive comments of two anonymous reviewers and the suggestions of Emmanuel Boss who helped to greatly improve the original manuscript.

References

Agrawal, Y., McCave I. and Riley J.: Laser diffraction size analysis, in Principles, Methods, and Application of Particle Size Analysis, edited by James P. M. Syvitski, pp. 119–129, Cambridge University Press, N. Y., 1991.

Agrawal, Y. C., A. Whitmire, O. A. Mikkelsen and H. C. Pottsmith H.C.: Light scattering by random shaped particles and consequences of measuring suspended sediments by laser diffraction, J. Geophys. Res., 113, C04023. doi:10.1029/2007JC004403, 2008.

Andrews, S., D. Nover and S. G. Schladow: Using laser diffraction data to obtain accurate particle size distributions: The role of particle composition, Limnol. Oceanogr.: Methods 8, 507–526. doi:10.4319/lom.2010.8.507, 2010.

Babin, M., Therriault, J.C., Legendre, L. and Condal, A.: Variations in the specific absorption coefficient for natural phytoplankton assemblages: Impact on estimates of primary production, Limnol. Oceanogr., 38, 154-177, 1993.

Babin, M., Stramski D., Ferrari G.M., Claustre H., Bricaud, A., Obolensky, G. and Hoepffner N.: Variations in the light absorption coefficients of phytoplankton, nonalgal particles, and dissolved organic matter in coastal waters around Europe, J. Geophys. Res., 108, 10.1029/2001JC000882, 2003.

Babin, M. and Stramski, D.: Variations in the mass-specific absorption coefficient of mineral particles suspended in water, Limnol. Oceanogr., 49, 756–767, 2004.

Barillé-Boyer, A.L., Barillé, L., Massé, H., Razet, D. and Héral, M: Correction for particulate organic matter as estimated by loss on ignition in estuarine ecosystems, Estuar. Coast. Shelf Sci., 58, 147–153, 2003.

Binding, C.E., Bowers, D.G. and Mitchelson-Jacob, E.G.: Estimating suspended sediment concentrations from ocean colour measurements in moderately turbid waters; the impact of variable particle scattering properties, Rem. Sens. Environ., 94, 373-383, 2005.

Boss, E., Twardowski, M.S., and Herring, S.: Shape of the particulate beam attenuation spectrum and its relation to the size distribution of oceanic particles, App. Opt. 40, 4885–4893, 2001.

Boss, E., Slade, H., Behrenfeld, M. and Dall'Olmo, G.: Acceptance angle effects on the beam attenuation in the ocean, Opt. Expr., 17, 1535-1550, 2009.

Boss, E., Picheral, M., Leeuwa, T., Chase, A., Karsenti, E., Gorsky, G., Taylor, L., Slade, W., Ras, J., Claustre, H.: The characteristics of particulate absorption, scattering and attenuation coefficients in the surface ocean; Contribution of the Tara Oceans expedition, Methods in oceanography, 7, 52-62, 2013.

Bowers, D. G. and Binding, C. E.: The optical properties of mineral suspended particles: A review and synthesis, Estuar. Coast. Shelf Sci., 67, 219–230, 2006.

Bowers, D.G., Braithwaite, K.M., Nimmo-Smith, W. A. M. and Graham, G. W.: Light scattering by particles suspended in the sea: The role of particle size and density, Cont. Shelf Res., 29, 1748–1755, 2009.

Bricaud, A. and Stramski, D.: Spectral absorption coefficients of living phytoplankton and nonalgal biogenous matter: A comparison between Peru upwelling area and the Sargasso Sea, Limnol. Oceanogr., 35, 562-582, 1990.

Chanut, J. P. and Poulet, S. A.: Short-term variability of the size spectra of suspended particles in a rapidly changing environment, Estuar. Coast. Shelf Sci., 15, 497–513, 1982.

D'Anglejan, B. F. and Smith, E. C.: Distribution, Transport, and Composition of Suspended Matter in the St. Lawrence Estuary, Can. J. Earth Sci., 10, 1380–1396, 1973.

Dalu, T., Richoux, N. B., and Froneman, P. W.: Nature and source of suspended particulate matter and detritus along an austral temperate river-estuary continuum, assessed using stable isotope analysis, Hydrobiologia, 767, 95-110, 2016.

Deflandre B., Mucci, A., Gagne, J.P., Guignard, C., Sundby, and B.: Early diagenetic processes in coastal marine sediments disturbed by a catastrophic sedimentation event. Geochimica et Cosmochimica Acta, 66, 2547-2558, 2002.

Devlin, M. J., Barry, J., Mills, D. K., Gowen, R. J., Foden, J., Sivyer, D., and Tett, P.: Relationships between suspended particulate material, light attenuation and Secchi depth in UK marine waters, Estuar. Coast. Res. Shelf Sci., 79, 429-439, 2008.

Doxaran, D., Froidefond, J. M., Lavender, S., and Castaing, P.: Spectral signature of highly turbid waters: Application with SPOT data to quantify suspended particulate matter concentrations, Remote Sens. Environ., 81, 149–161, 2002.

Doxaran, D., Ruddick, K., McKee, D., Gentili, B., Tailliez, D., Chami, M. and Babin, M.: Spectral variation of light scattering by marine paticles in coastal waters, from visible to near infrared, Limnol. Oceanogr., 54, 1257–1271, , 2009.

D'Sa E.J., Miller R.L., and Del Castillo C: Bio-optical properties and ocean color algorithms for coastal waters influenced by the Mississippi River during a cold front, Appl. Opt., 45, 7410–7428, 2006.

D'Sa E.J. and Ko, D.S.: Short-term influences on suspended particulate matter distribution in the Northern Gulf of Mexico: Satellite and model observations. Sensors, 8, 4249-4264, 2008.

Eleveld, M.A.,vand der Wal, D. and Van Kessel, T.: Estuarine suspended particulate matter concentrations from sun-synchronous satellite remote sensing:Tidal and meteorological effects and biases, Rem. Sens. of Environ., 143, 2014-215, 2014.

Estapa, M. L., Boss, E., Mayer, L. M. and Roesler, C. S.: Role of iron and organic carbon in mass-specific light absorption by particulate matter from Louisiana coastal waters, Limnol. Oceanogr., 57, 97–112, 2012.

Gagné, H., Lajeunesse, P., St-Onge, G. and Bolduc, A.: Recent transfer of coastal sediments to the Laurentian Channel, Lower St. Lawrence Estuary (Eastern Canada), through submarine canyon and fan systems, Geo-Marine Lett., 29, 191–200, 2009.

Guinder, V. A., Popovich, C. A., and Perillo, G. M. E.: Particulate suspended matter concentrations in the Bahia Blanca Estuary, Argentina: Implication for the development of phytoplankton blooms, Estuar. Coast. Res. Shelf Sci., 85, 157-165, 2009.

Larouche, P. and Boyer-Villemaire, U.: Suspended particulate matter in the St. Lawrence estuary and Gulf surface layer and development of a remote sensing algorithm, Estuar. Coast. Shelf Sci., 90, 241–249, 2010.

Levasseur, M., Therriault, J.-C. and Legendre, L.: Hierarchical control of phytoplankton succession by physical factors, Mar. Ecol. Prog. Ser., 19, 211–222, 1984.

Loisel, H., Nicolas, J. M., Sciandra, A., Stramski, D. and Poteau, A.: Spectral dependency of optical backscattering by marine particles from satellite remote sensing of the global ocean, J. Geophys. Res. Ocean., 111, 1–14, 2006.

Loisel, H., Duforet, L., Dessailly, D., Chami, M., and Dubuisson, P.: Investigation of the variations in the water leaving polarized reflectance from the POLDER satellite data over two biogeochemical contrasted oceanic areas, Opt. Exp., 17, 12905-12918, 2008.

Löptien, U. and Meier, H. E. M.: The influence of increasing water turbidity on the sea surface temperature in the Baltic Sea: A model sensitivity study, J. Mar. Syst., 88, 323–331, 2011.

Ma, H., Kim, S. D., Allen, H. E., and Cha, D. K.: Effect of copper binding by suspended particulate matter on toxicity, Environ. Toxicol. Chem. 21, 710-714, 2002.

Mayer, L.M.: Surface area control of organic carbon accumulation in continental shelf sediments. Geochim. Cosmochim. Acta, 58, 1271–1284, 1994.

McKee, D., Piskozub, J. and Brown, I.: Scattering error corrections for in situ absorption and attenuation measurements, Opt. Exp., 16, 19480-19492, 2008.

McKee, D., Piskozub, J., Röttgers, R., Reynolds, R.A.: Evaluation and improvement of an iterative scattering correction scheme for in situ absorption and attenuation measurements, J.Amer. Ocean. Technol.,30, doi.10.1175/JTECH-D-12-00150.1, 2013.

Miller, R. L. and McKee, B. A.: Using MODIS Terra 250 m imagery to map concentrations of total suspended matter in coastal waters, Remote Sens. Environ., 93, 259–266, 2004.

Mohammadpour, G., Montes-Hugo, M. A., Stavn, R., Gagné, J. P. and Larouche, P.: Particle Composition Effects on MERIS-Derived SPM: A Case Study in the Saint Lawrence Estuary, Can. J. Remote Sens., 41, 515–524, 2015.

Montes-Hugo, M. A. and Mohammadpour, G.: Biogeo-optical modeling of SPM in the St. Lawrence Estuary, Can. J. Remote Sens., 38, 197–209, 2012.

Morel, A. 1974: Optical properties of pure water and pure sea water, in Optical aspects of oceanography, edited by N.G. Jerlov, and Nielsen, E. S., pp. 1-24, Academic, New York, 1974.

Morel, A. and Antoine, D.: Heating Rate within the Upper Ocean in Relation to its Bio–optical State, J. Phys. Oceanogr., 24, 1652–1665, 1994.

Neukermans, G., Loisel, H., Mériaux, X., Astoreca, R. and McKee, D.: In situ variability of mass-specific beam attenuation and backscattering of marine particles with respect to particle size, density, and composition, Limnol. Oceanogr., 57, 124–144, 2012.

Neukermans, G., Reynolds, R. A. and Stramski, D.: Optical classification and characterization of marine particle assemblages within the western Arctic Ocean, Limnol. Oceanogr., 61, 1472–1494, 2016.

Nieke, B., Reuter, R., Heuermann, R., Wang, H., Babin, M. and Therriault, J. C.: Light absorption and fluorescence properties of chromophoric dissolved organic matter (CDOM), in the St. Lawrence Estuary (Case 2 waters), Cont. Shelf Res., 17, 235–252, 1997.

Pearson, R.K.: Mining imperfect data. Dealing with contamination and incomplete records. Society for Industrial and Applied Mathematics, 305 p. doi.org/10.1137/1.9780898717884, 2005.

Pegau, W.S., Gray, D., and Zaneveld, J.R.V.: Absorption and attenuation of visible and near-infrared light inwater: Dependence on temperature and salinity, Appl. Opt., 36, 6035–6046, 1997.

Pope, R., and Fry, E.: Absorption spectrum (380 - 700 nm) of pure waters: II. Integrating cavity measurements, Applied Optics, 36, 8710-8723, 1997.

Poulet, S., Cossa, D. and Marty, J.-C.: Combined analyses of the size spectra and biochemical composition of particles in the St. Lawrence estuary, Mar. Ecol. Prog. Ser., 30, 205–214, 1986.

Poulton, S.W., and Raiswell R.: Chemical and physical characteristics of iron oxides in riverine and glacial meltwater sediments, Chem. Geol., 218, 203-221, 2005.

Ramalhosa, E., Pereira, E., Vale, C., Válega, M., Monterroso, and P., Duarte, A. C.: Mercury distribution in Douro estuary (Portugal), Mar. Poll. Bull. 50, 1218-1222, 2005.

Reynolds, R.A., Stramski, D., Wright,V.M., and Woźniak, S.B.: Measurements and characterization of particle size distributions in coastal waters, J. Geoph. Res., 115, doi:10.1029/2009JC005930, 2010.

Reynolds, R. A., Stramski, D. and Neukermans, G.: Optical backscattering by particles in Arctic seawater and relationships to particle mass concentration, size distribution, and bulk composition, Limnol. Oceanogr., 61, 1869–1890, 2016.

Risovic, D.: Two component model of the sea particle size distribution, Deep-Sea Res., Part I, 40, 1459–1473, 1993.

Röttgers, R., Schönfeld, W., Kipp, P.R., and Doerffer, R.: Practical test of a point-source integrating cavity absorption meter: The performance of different collector assemblies, App. Opt., 44, 5549-5560, 2005.

Röttgers, R., McKee, D., and Woźniak, S. B.: Evaluation of scatter corrections for ac-9 absorption measurements in coastal waters, Methods Oceanogr., 7, 21–39, 2013.

Röttgers, R., Dupouy, C., Taylor, B. B., Bracher, A. and Woźniak, S. B.: Mass-specific light absorption coefficients of natural aquatic particles in the near-infrared spectral region, Limnol. Oceanogr., 59, 1449–1460, 2014.

Slade, W.H., Boss, E. and Russo C.: Effects of particle aggregation and disaggregation on their inherent optical properties, Opt. Exp., 19, 7945-7959, 2011.

Snyder, W., Arnone, R., Davis, C. O., Goode, W., Gould, R. W., Ladner, S., Lamela, G., Rhea, W. J., Stavn, R., Sydor, M. and Weidemann, A.: Optical scattering and backscattering by organic and inorganic particulates in U.S. coastal waters., Appl. Opt., 47, 666–77, 2008.

Spearman, C.: The Proof and Measurement of Association between two things, The Amer. J. of Psych. , 15 , 1904.

Stavn, R. H. and Richter, S. J.: Biogeo-optics: particle optical properties and the partitioning of the spectral scattering coefficient of ocean waters, Appl. Opt., 47, 2660–2679, 2008.

Strickland, J.D.H. and Parsons, T.R.: A practical handbook of seawater analysis. Fisheries Research Board Canada, 310 p., 1972.

Tremblay, L. and Gagné, J. P.: Distribution and biogeochemistry of sedimentary humic substances in the St. Lawrence Estuary and the Saguenay Fjord, Québec, Org. Geochem., 38, 682–699, 2007.

Tremblay, L. and Gagné, J. P.: Organic matter distribution and reactivity in the waters of a large estuarine system, Mar. Chem., 116, 1–12, 2009.

Twardowski, M.S., Boss, E., Macdonald, J.B., Pegau, W.S., Barnard, A.H. and Zaneveld J.R.V.: A model for estimating bulk refractive index from the optical backscattering ratio and the implications for understanding particle composition in case I and case II waters, J. Geophy. Res, 106, C7, 14,129-14,142, 2001.

Woźniak, S. B., Stramski, D., Stramska, M., Reynolds, R. A., Wright, V. M., Miksic, E. Y., Cichocka, M. and Cieplak, A. M.: Optical variability of seawater in relation to particle concentration, composition, and size distribution in the nearshore marine environment at Imperial Beach, California, J. Geophys. Res. Ocean., 115, 1–19, 2010.

Xi, H., Larouche, P., Tang, S. and Michel, C.: Seasonal variability of light absorption properties and water optical constituents in Hudson Bay, Canada, J. Geophys. Res. Ocean., 118, 3087–3102, 2014.

Xie, H., Aubry C., Bélanger S., and Song G.: The dynamics of absorption coefficients of CDOM and particles in the St. Lawrence estuarine system: Biogeochemical and physical implications, Mar. Chem., 128-129, 44-56, 2012.

Yeats, P. A.: The distribution of trace metals in ocean waters, Sci. Total Environ., 72, 131–149, 1988.

Yeats, P. A. and Bewers, J. M.: Trace metals in the waters of the Saguenay Fjord, Can. J. Earth Sci., 13, 1319–1327, 1976.

Zaneveld, J.R.V., Kitchen, J.C., Moore, C.M.: The scattering correction error of the reflecting-tube absorption meters, Ocean Optics XII, J.S. Jaffe, Ed. International Society for Optical Engineering, SPIE proceedings, vol. 2258, 44-58, 1994.

Zhang, X., Huot, Y., Gray, D.J.,Weidemann, A., and Rhea,W.J.: Biogeochemical origins of particles obtained from the inversion of the volume scattering function and spectral absorption in coastal waters, Biogeosciences, 10, 6029e6043, 2013.

Zhang, X., Stavn, R. H., Falster, A. U., Gray, D. and Gould, R. W.: New insight into particulate mineral and organic matter in coastal ocean waters through optical inversion, Estuar. Coast. Res. Shelf Sci., 149, 1–12, 2014.

Zhang, X., Stavn, R.H., Falster, A.U., Rick, J.J., Gray, D. and R.W. Gould, Jr.: Size distributions of coastal ocean suspended particulate inorganic matter:Amorphous silica and clay minerals and their dynamics, Estuar., Coast. Shelf Sci.. DOI: 10.1016/j.ecss.2017.03.025, 2017.

Table 1. Summary of acronyms

Abbreviation	Definition	Unit
SLE	St. Lawrence Estuary	
UE	Upper estuary	
SF	Saguenay Fjord	
LE	Lower estuary	
POM	Particulate organic matter	
PIM	Particulate inorganic matter	
PSD	Particle size distribution	
F_{SPM}^{i}	Contribution of size fraction i to total mass of SPM	dimensionless
F_{SPM}^{j}	Contribution of chemical fraction j to total mass of SPM	dimensionless
NAP	Non-algal particulates	
CDOM	Chromophoric dissolved organic matter	
λ	Light wavelength	nm
a_{SPM}	Absorption coefficient of total SPM	m^{-1}
b_{SPM}	Scattering coefficient of total SPM	m^{-1}
c_{SPM}	Particulate beam attenuation coefficient of total SPM	m^{-1}
a_{SPM}^{*}	Mass-specific absorption coefficient of total SPM	$m^2\ g^{-1}$
b_{SPM}^{*}	Mass-specific scattering coefficient of total SPM	$m^2\ g^{-1}$
ξ	Power-law exponent of the exponential fit to the differential particle size distribution	Number of particulates per µm

D	Diameter of a volume-equivalent sphere at mid-point of size class	µm
V(D)	Volume concentration at size class D	µL L^{-1}
N(D)	Particle number concentration at size class D	m^{-3}
N'(D)	Particle number density at size class D	m^{-3} $µm^{-1}$
γ	Spectral slope of particulate beam attenuation coefficient	nm^{-1}
Svis	Spectral slope of mass-specific particulate absorption coefficient within the visible spectral range	nm^{-1}

Table 2. Particle size and chemical composition effects on mass-specific optical coefficients. Spearman rank correlations for a_i^* and b_i^* are computed at a wavelength of 440 and 550 nm, respectively.

Mass-specific Optical fraction	ξ	F_{SPM}^{PIM}
$a_{0.2-0.4\ \mu m}^*$	0.32 *	0.31 *
$a_{0.4-0.7\ \mu m}^*$	0.28 *	0.50 **
$a_{0.7-10\ \mu m}^*$	0.26 *	0.49 *
$a_{>10\ \mu m}^*$	0.31 *	0.44 *
$b_{0.2-0.4\ \mu m}^*$	0.15	-0.17 *
$b_{0.4-0.7\ \mu m}^*$	0.05	-0.06
$b_{0.7-10\ \mu m}^*$	0.23 *	0.42 *
$b_{>10\ \mu m}^*$	0.37 *	0.26 *

Table 3. Correlation of optical proxies with mass-derived size and chemical fractions of SPM. Spearman rank correlations based on 23 samples.

Mass fraction	γ	*Svis*
F_{SPM}^{PIM}	-0.34	-0.06
$F_{SPM}^{0.2\text{-}0.4\ \mu m}$	0.53*	0.49**
$F_{SPM}^{0.4\text{-}0.7\ \mu m}$	-0.43*	-0.49**
$F_{SPM}^{0.7\text{-}10\ \mu m}$	-0.38*	-0.30*
$F_{SPM}^{>10\ \mu m}$	0.13	0.19

Table 4. Mass-specific optical coefficients of suspended particulates for different littoral environments. Acronyms and units are defined in Table 1.

Location	λ	a_{SPM}^*	b_{SPM}^*	[SPM] [k]	References
UE	440	0.01 – 0.25[a]	0.01 – 1.06 [a]	2.28 – 30.6	This study
	488	0.01 – 0.14	0.01 – 0.97		
	556	0.01 – 0.06	0.01 – 0.86		
	665	0.01 – 0.02	0.01 – 0.73		
	708	0.01 – 0.012	0.01 – 0.68		
SF	440	0.32 - 0.73	0.20-0.56		
	488	0.17 - 0.39	0.18-0.49		
	556	0.08 – 0.17	0.15-0.42		
	665	0.02 – 0.04	0.13 – 0.34		
	708	0.01 – 0.02	0.12 – 0.31		
LE	440	0.03 – 0.07	0.04 – 0.22		
	488	0.02 – 0.04	0.04 – 0.21		
	556	0.01 – 0.02	0.04 – 0.19		
	665	0.003 – 0.006	0.04 – 0.18		

	708	0.015 – 0.002	0.04 – 0.17		
Elber River,	650	0.001 – 0.020[b]		0.5-10	Röttgers et al. (2014)
German Bight,	750	0.001 – 0.019			
Baltic Sea, New Caledonia lagoon	850	0.001 – 0.014			
Monterey Bay, US	532		0.46 – 2.54[c]	0.11 – 2.37	Zhang et al. (2014)
Mobile Bay, US	532		0.40 – 1.78	0.26 – 7.36	
Mobile Bay,	440	0.44 – 1.95[d]		0.23-25.32	Stavn and Richter (2008)
Southwest Pass, US	488	0.41 – 1.89			
	550	0.40 – 1.80			
	676	0.36 – 1.63			
	715	0.34 – 1.61			
Coast of New Jersey,	440			0.44 – 6.6	Snyder et al. (2008)
Monterey Bay,	488				
Great Bay	556				
Mobile Bay	665	0.05 ± 0.01[d] (arithmetic			

		mean ± standard deviation)			
Irish sea, UK	665		0.08 – 0.45[e]	1.9 – 26.5	Binding et al. (2005)
Irish sea, UK	443	0.062 ± 0.013[f]	0.17 – 0.19	1.6 – 50	Bowers and Binding (2006)
	490		0.20 – 0.22		
	555		0.20 – 0.24		
	665		0.14 – 0.15		
Coast off Europe and French Guyana	676		0.63 – 2.07[g]	1.2 – 82.4	Neukermans et al. (2012)
Elbe Estuary, Germany	555	0.05 – 0.07 [d]	0.35 – 0.47	73.5 – 294.2	Doxaran et al. (2009)
	715	0.01 – 0.03	0.32 – 0.44		
Gironde Estuary, France	555	0.02 – 0.06	0.28 – 0.50	21.9 – 344.1	
	715	0.01 – 0.02	0.27 – 0.45		
Coastal Louisiana and lower Atchafalaya and Mississsippi Rivers	440	0.056 ± 0.012[g] (0.05 - 0.065)			Estapa et al. (2012)

	488	0.035 - 0.05			
	556	0.25 - 0.35			
	665	0.125 - 0.02			
West of Mississippi Delta	443	0.01 2 -0.079 [d]			D'Sa et al. (2006)
Imperial Beach, California	440	0.03 – 0.1[h]	0.1 - 1.2	3-90	Wozniak et al. (2010)
	488	0.02 – 0.08	0.18 - 0.9		
	556	0.01 – 0.03	0.2 - 0.9		
	665	0.004 - 0.02	0.2 - 0.8		
	708	0.001 - 0.02	0.2 - 0.8		

[a]ac-s measurements and sum of weights of SPM size fractions 0.2-0.4 μm, 0.4-0.7 μm, 0.7-10 μm and >10 μm, [b]integrating sphere coupled to spectrophotometer for suspensions and pad-technique, SPM weight based on GF/F (pore size = 0.7 μm) and nucleopore Whatman (pore size = 0.4 μm) filters, [c]Multispectral volume scattering meter and optical models for different particle subpopulations with assymetrical shape, [d]ac-9 measurements and SPM weight based on GF/F filters, [e]Irradiance meter PRR600 and optical models for estimating inherent optical properties and SPM weight based on GF/F filters, [f]comparable to [e]but pad-technique for estimating absorption coefficients of SPM, [g]comparable to [d] but using ac-s measurements, [g] comparable to [b] but using only suspensions and weight based on GF/F filters, [h]comparable to [b] but using only GF/F filters for SPM weight, [k]concentration of SPM in g m^{-3} and for particulates retained in glass-fiber filters with a pore size of 0.7 μm.

Figure captions

Figure 1. Study area. UE (red triangles), SF (green circles) and LE (blue rectangles). GSL is the Gulf of St. Lawrence.

Figure 2. Spectral variation of mass-specific optical coefficients for total SPM. (a) a_{SPM}^* and (b) b_{SPM}^*. Each bar is the arithmetic average ± 2 standard errors as computed for SLE-SF (black circles), UE (red circles), SF (green circles) and LE (blue circles). The number of observations for UE, SF and LE are 3, 5 and 15 respectively.

Figure 3. Spectral variation of mass-specific absorption coefficients for different size classes of suspended particulates. (a) 0.2-0.4 μm, (b) 0.4-0.7 μm, (c) 0.7-10 μm and (d) >10 μm. Color coding of symbols idem as Fig. 2. Curves presenting negative values at some wavelengths are not depicted.

Figure 4. Spectral variation of mass-specific scattering coefficients for different size classes of suspended particulates. Size classes and color coding of symbols idem as Fig. 3. Curves presenting negative values at some wavelengths are not depicted.

Figure 5. Spectral variation of mass-specific optical coefficients of SPM averaged over the entire study area. (a) a_i^* and (b) b_i^*. . Each bar is the arithmetic average ± 2 standard errors as computed for the size fractions 0.2-0.4 μm (solid symbol) and >10 μm (empty symbol).

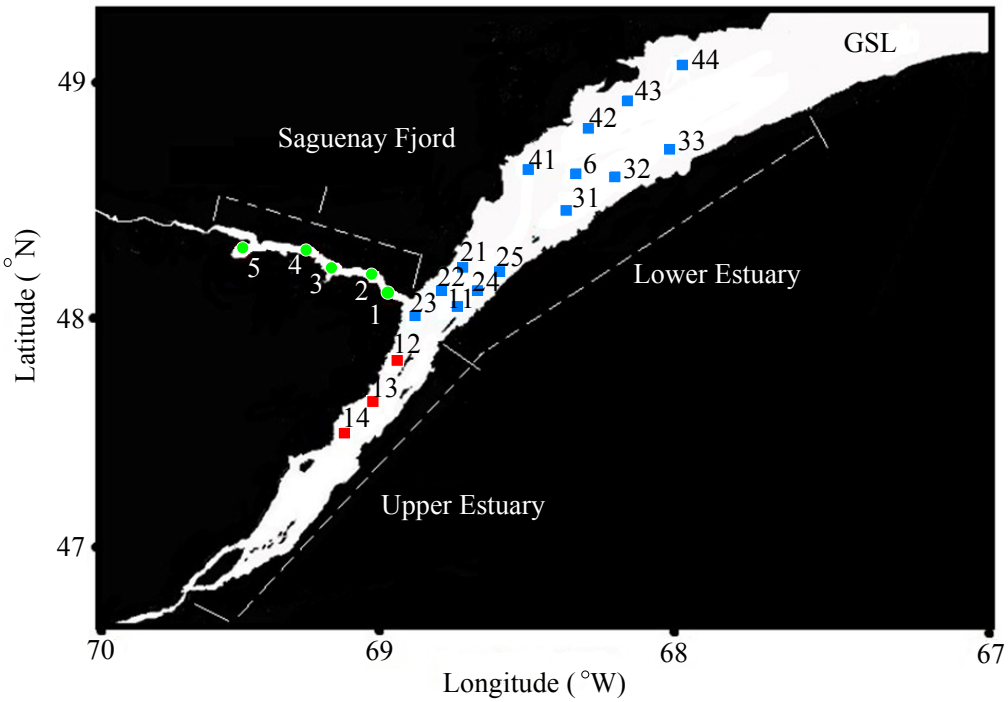
GSL
Saguenay Fjord
Lower Estuary
Upper Estuary
44
43
42
33
41
6
32
31
21
25
22
24
11
23
5
4
3
2
1
12
13
14
49
48
47
70
69
68
67
Latitude (°N)
Longitude (°W)

fig. 1

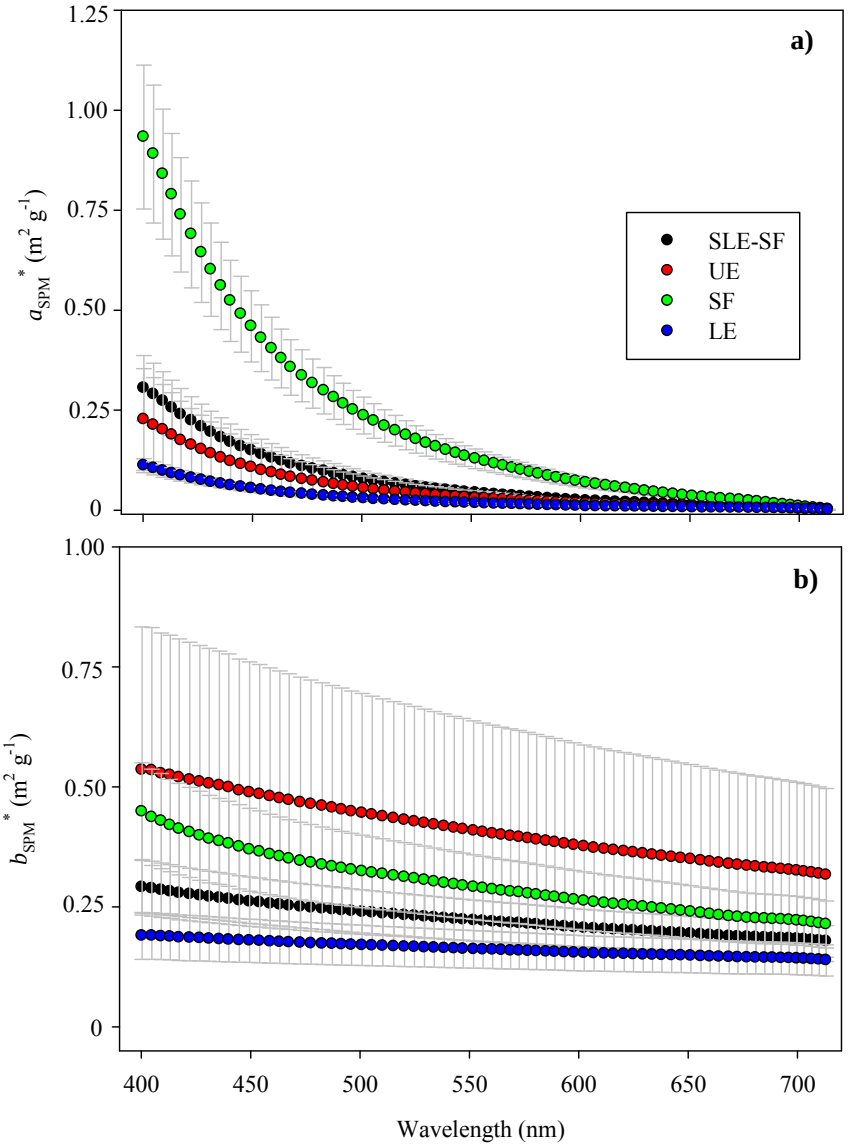
a)
b)
SLE-SF
UE
SF
LE
a_{SPM}^{*} (m^2 g^{-1})
b_{SPM}^{*} (m^2 g^{-1})
1.25
1.00
0.75
0.50
0.25
0
400
450
500
550
600
650
700
Wavelength (nm)

Fig. 2

5

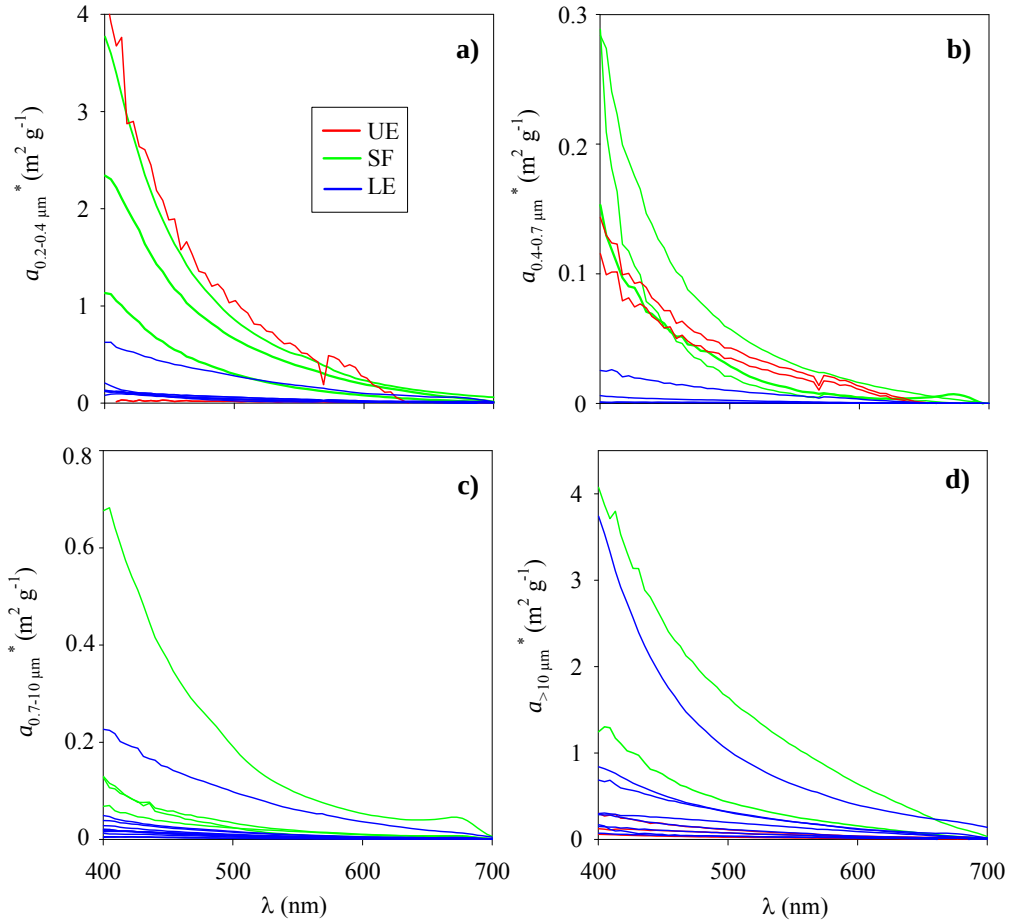
a)
b)
c)
d)
UE
SF
LE
$a^*_{0.2\text{-}0.4\,\mu m}$ (m^2 g^{-1})
$a^*_{0.4\text{-}0.7\,\mu m}$ (m^2 g^{-1})
$a^*_{0.7\text{-}10\,\mu m}$ (m^2 g^{-1})
$a^*_{>10\,\mu m}$ (m^2 g^{-1})
λ (nm)
λ (nm)

Fig. 3

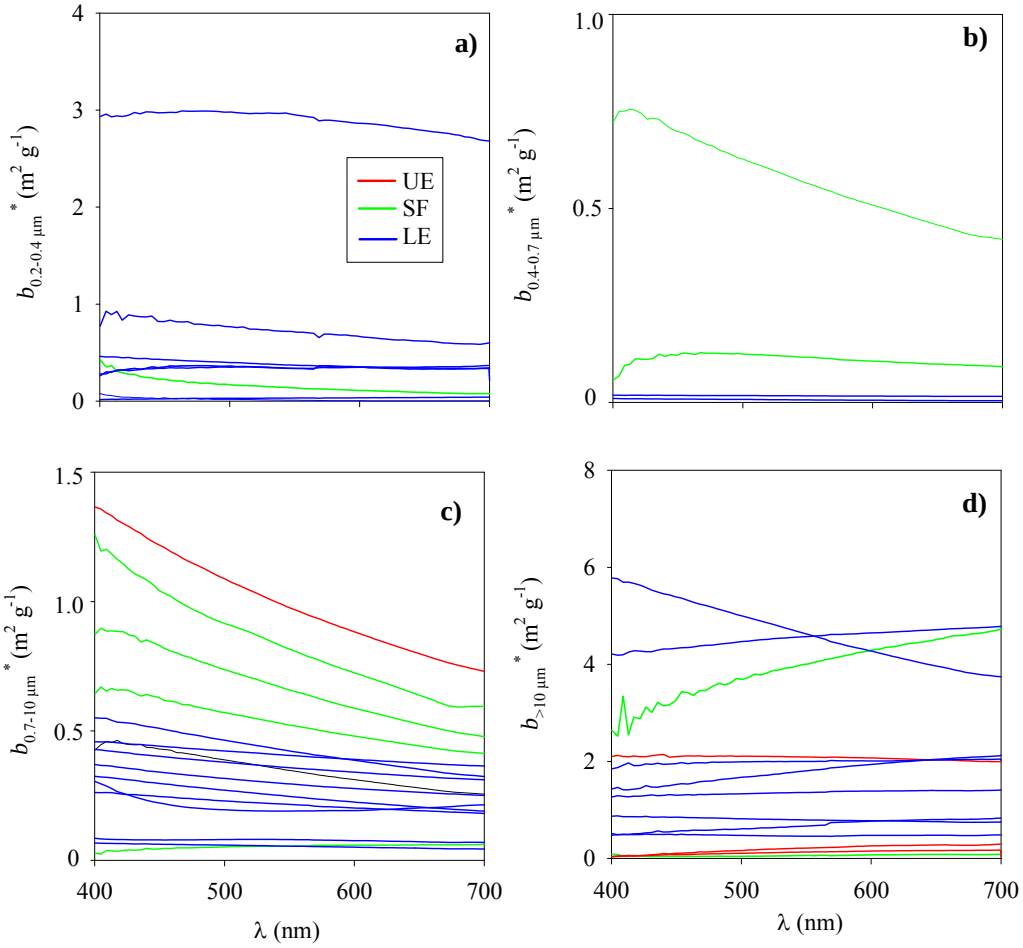
a)
b)
c)
d)
UE
SF
LE
$b^*_{0.2\text{-}0.4\,\mu m}$ (m^2 g^{-1})
$b^*_{0.4\text{-}0.7\,\mu m}$ (m^2 g^{-1})
$b^*_{0.7\text{-}10\,\mu m}$ (m^2 g^{-1})
$b^*_{>10\,\mu m}$ (m^2 g^{-1})
λ (nm)
λ (nm)

5 Fig. 4

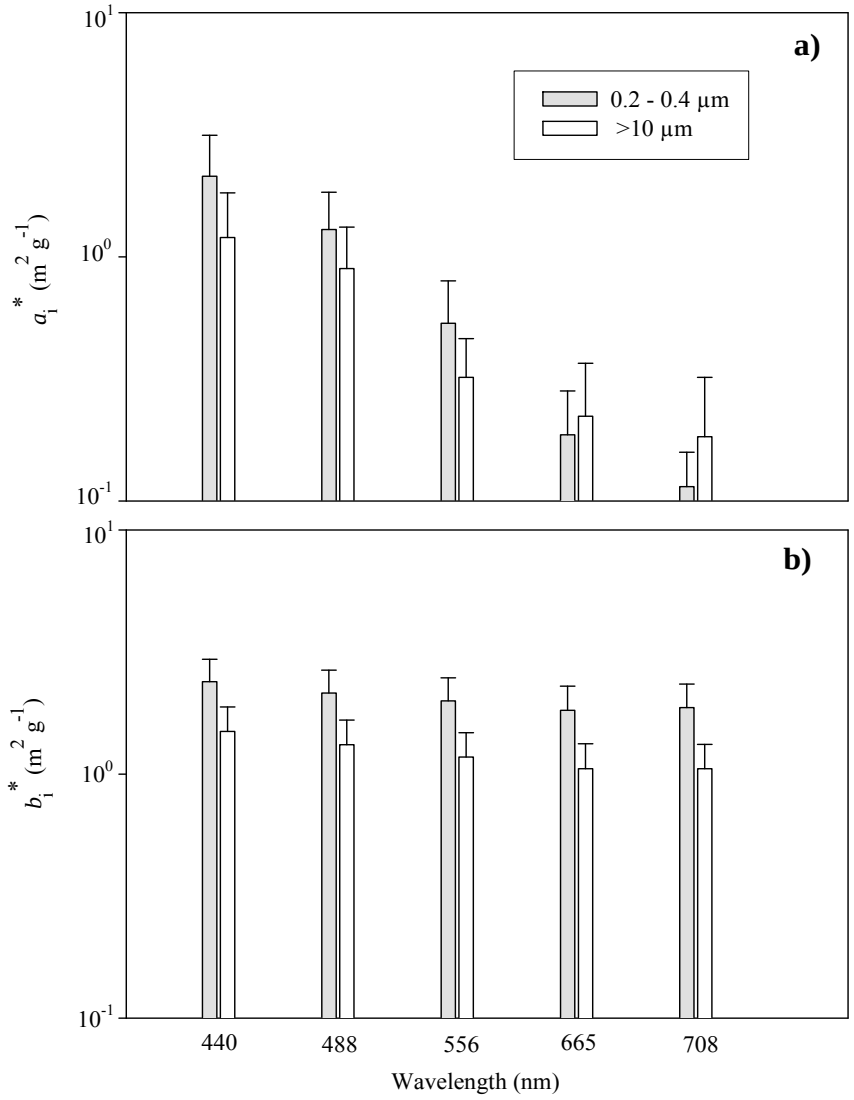
a)
0.2 - 0.4 µm
>10 µm
a_i^* (m^2 g^{-1})
10^1
10^0
10^{-1}
b)
b_i^* (m^2 g^{-1})
440
488
556
665
708
Wavelength (nm)

fig. 5

5